

Observation of a Near-Threshold Structure in the K^+ Recoil-Mass Spectra in
 $e^+e^- \rightarrow K^+(D_s^- D^{*0} + D_s^{*-} D^0)$

M. Ablikim¹, M. N. Achasov^{10,c}, P. Adlarson⁶⁷, S. Ahmed¹⁵, M. Albrecht⁴, R. Aliberti²⁸, A. Amoroso^{66A,66C}, Q. An^{63,50}, Anita²¹, X. H. Bai⁵⁷, Y. Bai⁴⁹, O. Bakina²⁹, R. Baldini Ferroli^{23A}, I. Balossino^{24A}, Y. Ban^{39,k}, K. Begzsuren²⁶, N. Berger²⁸, M. Bertani^{23A}, D. Bettini^{24A}, F. Bianchi^{66A,66C}, J. Biernat⁶⁷, J. Bloms⁶⁰, A. Bortone^{66A,66C}, I. Boyko²⁹, R. A. Briere⁵, H. Cai⁶⁸, X. Cai^{1,50}, A. Calcaterra^{23A}, G. F. Cao^{1,55}, N. Cao^{1,55}, S. A. Cetin^{54B}, J. F. Chang^{1,50}, W. L. Chang^{1,55}, G. Chelkov^{29,b}, D. Y. Chen⁶, G. Chen¹, H. S. Chen^{1,55}, M. L. Chen^{1,50}, S. J. Chen³⁶, X. R. Chen²⁵, Y. B. Chen^{1,50}, Z. J. Chen^{20,l}, W. S. Cheng^{66C}, G. Cibinetto^{24A}, F. Cossio^{66C}, X. F. Cui³⁷, H. L. Dai^{1,50}, X. C. Dai^{1,55}, A. Dbeysy¹⁵, R. B. de Boer⁴, D. Dedovich²⁹, Z. Y. Deng¹, A. Denig²⁸, I. Denysenko²⁹, M. Destefanis^{66A,66C}, F. De Mori^{66A,66C}, Y. Ding³⁴, C. Dong³⁷, J. Dong^{1,50}, L. Y. Dong^{1,55}, M. Y. Dong^{1,50,55}, X. Dong⁶⁸, S. X. Du⁷¹, J. Fang^{1,50}, S. S. Fang^{1,55}, Y. Fang¹, R. Farinelli^{24A}, L. Fava^{66B,66C}, F. Feldbauer⁴, G. Felici^{23A}, C. Q. Feng^{63,50}, M. Fritsch⁴, C. D. Fu¹, Y. Fu¹, Y. Gao^{39,k}, Y. Gao⁶⁴, Y. Gao^{63,50}, Y. G. Gao⁶, I. Garzia^{24A,24B}, E. M. Gersabeck⁵⁸, A. Gilman⁵⁹, K. Goetzen¹¹, L. Gong³⁴, W. X. Gong^{1,50}, W. Gradl²⁸, M. Greco^{66A,66C}, L. M. Gu³⁶, M. H. Gu^{1,50}, S. Gu², Y. T. Gu¹³, C. Y. Guan^{1,55}, A. Q. Guo²², L. B. Guo³⁵, R. P. Guo⁴¹, Y. P. Guo^{9,h}, Y. P. Guo²⁸, A. Guskov²⁹, T. T. Han⁴², X. Q. Hao¹⁶, F. A. Harris⁵⁶, K. L. He^{1,55}, F. H. Heinsius⁴, C. H. Heinz²⁸, T. Held⁴, Y. K. Heng^{1,50,55}, C. Herold⁵², M. Himmelreich^{11,f}, T. Holtmann⁴, Y. R. Hou⁵⁵, Z. L. Hou¹, H. M. Hu^{1,55}, J. F. Hu^{48,m}, T. Hu^{1,50,55}, Y. Hu¹, G. S. Huang^{63,50}, L. Q. Huang⁶⁴, X. T. Huang⁴², Y. P. Huang¹, Z. Huang^{39,k}, N. Huesken⁶⁰, T. Hussain⁶⁵, W. Ikegami Andersson⁶⁷, W. Imoehl²², M. Irshad^{63,50}, S. Jaeger⁴, S. Janchiv^{26,j}, Q. Ji¹, Q. P. Ji¹⁶, X. B. Ji^{1,55}, X. L. Ji^{1,50}, H. B. Jiang⁴², X. S. Jiang^{1,50,55}, X. Y. Jiang³⁷, Y. Jiang⁵⁵, J. B. Jiao⁴², Z. Jiao¹⁸, S. Jin³⁶, Y. Jin⁵⁷, T. Johansson⁶⁷, N. Kalantar-Nayestanaki³¹, X. S. Kang³⁴, R. Kappert³¹, M. Kavatsyuk³¹, B. C. Ke^{44,1}, I. K. Keshk⁴, A. Khoukaz⁶⁰, P. Kiese²⁸, R. Kiuchi¹, R. Kliemt¹¹, L. Koch³⁰, O. B. Kolcu^{54B,e}, B. Kopf⁴, M. Kuemmel⁴, M. Kuessner⁴, A. Kupsch⁶⁷, M. G. Kurth^{1,55}, W. Kuhn³⁰, J. J. Lane⁵⁸, J. S. Lange³⁰, P. Larin¹⁵, L. Lavezzi^{66A,66C}, Z. H. Lei^{63,50}, H. Leithoff²⁸, M. Lellmann²⁸, T. Lenz²⁸, C. Li⁴⁰, C. H. Li³³, Cheng Li^{63,50}, D. M. Li⁷¹, F. Li^{1,50}, G. Li¹, H. Li⁴⁴, H. Li^{63,50}, H. B. Li^{1,55}, H. J. Li^{9,h}, J. L. Li⁴², J. Q. Li⁴, Ke Li¹, L. K. Li¹, Lei Li³, P. L. Li^{63,50}, P. R. Li^{32,n,o}, S. Y. Li⁵³, W. D. Li^{1,55}, W. G. Li¹, X. H. Li^{63,50}, X. L. Li⁴², Z. Y. Li⁵¹, H. Liang^{63,50}, H. Liang^{1,55}, Y. F. Liang⁴⁶, Y. T. Liang²⁵, L. Z. Liao^{1,55}, J. Libby²¹, C. X. Lin⁵¹, B. J. Liu¹, C. X. Liu¹, D. Liu^{63,50}, F. H. Liu⁴⁵, Fang Liu¹, Feng Liu⁶, H. B. Liu¹³, H. M. Liu^{1,55}, Huanhuan Liu¹, Huihui Liu¹⁷, J. B. Liu^{63,50}, J. Y. Liu^{1,55}, K. Liu¹, K. Y. Liu³⁴, Ke Liu⁶, L. Liu^{63,50}, M. H. Liu^{9,h}, Q. Liu⁵⁵, S. B. Liu^{63,50}, Shuai Liu⁴⁷, T. Liu^{1,55}, W. M. Liu^{63,50}, X. Liu³², Y. Liu³², Y. B. Liu³⁷, Z. A. Liu^{1,50,55}, Z. Q. Liu⁴², X. C. Lou^{1,50,55}, F. X. Lu¹⁶, H. J. Lu¹⁸, J. D. Lu^{1,55}, J. G. Lu^{1,50}, X. L. Lu¹, Y. Lu¹, Y. P. Lu^{1,50}, C. L. Luo³⁵, M. X. Luo⁷⁰, P. W. Luo⁵¹, T. Luo^{9,h}, X. L. Luo^{1,50}, S. Lusso^{66C}, X. R. Lyu⁵⁵, F. C. Ma³⁴, H. L. Ma¹, L. L. Ma⁴², M. M. Ma^{1,55}, Q. M. Ma¹, R. Q. Ma^{1,55}, R. T. Ma⁵⁵, X. N. Ma³⁷, X. X. Ma^{1,55}, X. Y. Ma^{1,50}, F. E. Maas¹⁵, M. Maggiora^{66A,66C}, S. Maldaner²⁸, S. Malde⁶¹, Q. A. Malik⁶⁵, A. Mangoni^{23B}, Y. J. Mao^{39,k}, Z. P. Mao¹, S. Marcello^{66A,66C}, Z. X. Meng⁵⁷, J. G. Messchendorp³¹, G. Mezzadri^{24A}, T. J. Min³⁶, R. E. Mitchell²², X. H. Mo^{1,50,55}, Y. J. Mo⁶, N. Yu. Muchnoi^{10,c}, H. Muramatsu⁵⁹, S. Nakhoul^{11,f}, Y. Nefedov²⁹, F. Nerling^{11,f}, I. B. Nikolaev^{10,c}, Z. Ning^{1,50}, S. Nisar^{8,i}, S. L. Olsen⁵⁵, Q. Ouyang^{1,50,55}, S. Pacetti^{23B,23C}, X. Pan⁹, Y. Pan⁵⁸, A. Pathak¹, P. Patteri^{23A}, M. Pelizaeus⁴, H. P. Peng^{63,50}, K. Peters^{11,f}, J. Pettersson⁶⁷, J. L. Ping³⁵, R. G. Ping^{1,55}, A. Pitka⁴, R. Poling⁵⁹, V. Prasad^{63,50}, H. Qi^{63,50}, H. R. Qi⁵³, K. H. Qi²⁵, M. Qi³⁶, T. Y. Qi⁹, T. Y. Qi², S. Qian^{1,50}, W. B. Qian⁵⁵, Z. Qian⁵¹, C. F. Qiao⁵⁵, L. Q. Qin¹², X. S. Qin⁴², Z. H. Qin^{1,50}, J. F. Qiu¹, S. Q. Qu³⁷, K. H. Rashid⁶⁵, K. Ravindran²¹, C. F. Redmer²⁸, A. Rivetti^{66C}, V. Rodin³¹, M. Rolo^{66C}, G. Rong^{1,55}, Ch. Rosner¹⁵, M. Rump⁶⁰, H. S. Sang⁶³, A. Sarantsev^{29,d}, Y. Schelhaas²⁸, C. Schnier⁴, K. Schoenning⁶⁷, M. Scodreggio^{24A}, D. C. Shan⁴⁷, W. Shan¹⁹, X. Y. Shan^{63,50}, M. Shao^{63,50}, C. P. Shen⁹, P. X. Shen³⁷, X. Y. Shen^{1,55}, B. A. Shi⁵⁵, H. C. Shi^{63,50}, R. S. Shi^{1,55}, X. Shi^{1,50}, X. D. Shi^{63,50}, W. M. Song^{27,1}, Y. X. Song^{39,k}, S. Sosio^{66A,66C}, S. Spataro^{66A,66C}, K. X. Su⁶⁸, F. F. Sui⁴², G. X. Sun¹, H. K. Sun¹, J. F. Sun¹⁶, L. Sun⁶⁸, S. S. Sun^{1,55}, T. Sun^{1,55}, W. Y. Sun³⁵, X. Sun^{20,l}, Y. J. Sun^{63,50}, Y. K. Sun^{63,50}, Y. Z. Sun¹, Z. T. Sun¹, Y. H. Tan⁶⁸, Y. X. Tan^{63,50}, C. J. Tang⁴⁶, G. Y. Tang¹, J. Tang⁵¹, Y. J. X. Tang^{63,50}, V. Thoren⁶⁷, I. Uman^{54D}, C. W. Wang³⁶, D. Y. Wang^{39,k}, H. J. Wang⁵⁵, H. P. Wang^{1,55}, K. Wang^{1,50}, L. L. Wang¹, M. Wang⁴², M. Z. Wang^{39,k}, Meng Wang^{1,55}, W. H. Wang⁶⁸, W. P. Wang^{63,50}, X. Wang^{39,k}, X. F. Wang³², X. L. Wang^{9,h}, Y. Wang⁵¹, Y. Wang^{63,50}, Y. D. Wang³⁸, Y. F. Wang^{1,50,55}, Y. Q. Wang¹, Z. Wang^{1,50}, Z. Y. Wang¹, Ziyi Wang⁵⁵, Zongyuan Wang^{1,55}, D. H. Wei¹², P. Weidenkaff²⁸, F. Weidner⁶⁰, S. P. Wen¹, D. J. White⁵⁸, U. Wiedner⁴, G. Wilkinson⁶¹, M. Wolke⁶⁷, L. Wollenberg⁴, J. F. Wu^{1,55}, L. H. Wu¹, L. J. Wu^{1,55}, X. Wu^{9,h}, Z. Wu^{1,50}, L. Xia^{63,50}, H. Xiao^{9,h}, S. Y. Xiao¹, Y. J. Xiao^{1,55}, Z. J. Xiao³⁵, X. H. Xie^{39,k}, Y. G. Xie^{1,50}, Y. H. Xie⁶, T. Y. Xing^{1,55}, G. F. Xu¹, J. J. Xu³⁶, Q. J. Xu¹⁴, W. Xu^{1,55}, X. P. Xu⁴⁷, Y. C. Xu⁵⁵, F. Yan^{9,h}, L. Yan^{66A,66C}, L. Yan^{9,h}, W. B. Yan^{63,50}, W. C. Yan⁷¹, Xu Yan⁴⁷, H. J. Yang^{43,g}, H. X. Yang¹, L. Yang⁴⁴, R. X. Yang^{63,50}, S. L. Yang⁵⁵, S. L. Yang^{1,55}, Y. H. Yang³⁶, Y. X. Yang¹², Yifan Yang^{1,55}, Zhi Yang²⁵, M. Ye^{1,50}, M. H. Ye⁷, J. H. Yin¹, Z. Y. You⁵¹, B. X. Yu^{1,50,55}, C. X. Yu³⁷, G. Yu^{1,55}, J. S. Yu^{20,l}, T. Yu⁶⁴, C. Z. Yuan^{1,55}, L. Yuan², W. Yuan^{66A,66C}, X. Q. Yuan^{39,k}, Y. Yuan¹, Z. Y. Yuan⁵¹, C. X. Yue³³, A. Yuncu^{54B,a}, A. A. Zafar⁶⁵, Y. Zeng^{20,l}, B. X. Zhang¹, Guangyi Zhang¹⁶, H. Zhang⁶³, H. H. Zhang⁵¹, H. Y. Zhang^{1,50}, J. J. Zhang⁴⁴, J. L. Zhang⁶⁹, J. Q. Zhang⁴, J. W. Zhang^{1,50,55}, J. Y. Zhang¹, J. Z. Zhang^{1,55}, Jianyu Zhang^{1,55}, Jiawei Zhang^{1,55}, Lei Zhang³⁶, S. Zhang⁵¹, S. F. Zhang³⁶, Shulei Zhang^{20,l}, X. D. Zhang³⁸, X. Y. Zhang⁴², Y. Zhang⁶¹, Y. H. Zhang^{1,50}, Y. T. Zhang^{63,50}, Yan Zhang^{63,50}, Yao Zhang¹, Yi Zhang^{9,h}, Z. H. Zhang⁶, Z. Y. Zhang⁶⁸, G. Zhao¹, J. Zhao³³, J. Y. Zhao^{1,55}, J. Z. Zhao^{1,50}, Lei Zhao^{63,50}, Ling Zhao¹, M. G. Zhao³⁷, Q. Zhao¹, S. J. Zhao⁷¹, Y. B. Zhao^{1,50}, Y. X. Zhao²⁵, Z. G. Zhao^{63,50}, A. Zhemchugov^{29,b}, B. Zheng⁶⁴, J. P. Zheng^{1,50}, Y. Zheng^{39,k}, Y. H. Zheng⁵⁵, B. Zhong³⁵, C. Zhong⁶⁴, L. P. Zhou^{1,55}, Q. Zhou^{1,55}, X. Zhou⁶⁸, X. K. Zhou⁵⁵, X. R. Zhou^{63,50}, A. N. Zhu^{1,55}, J. Zhu³⁷, K. Zhu¹, K. J. Zhu^{1,50,55}, S. H. Zhu⁶², T. J. Zhu⁶⁹, W. J. Zhu³⁷, X. L. Zhu⁵³, Y. C. Zhu^{63,50}, Z. A. Zhu^{1,55}, B. S. Zou¹, J. H. Zou¹

(BESIII Collaboration)

- ¹ Institute of High Energy Physics, Beijing 100049, People's Republic of China
- ² Beihang University, Beijing 100191, People's Republic of China
- ³ Beijing Institute of Petrochemical Technology, Beijing 102617, People's Republic of China
- ⁴ Bochum Ruhr-University, D-44780 Bochum, Germany
- ⁵ Carnegie Mellon University, Pittsburgh, Pennsylvania 15213, USA
- ⁶ Central China Normal University, Wuhan 430079, People's Republic of China
- ⁷ China Center of Advanced Science and Technology, Beijing 100190, People's Republic of China
- ⁸ COMSATS University Islamabad, Lahore Campus, Defence Road, Off Raiwind Road, 54000 Lahore, Pakistan
- ⁹ Fudan University, Shanghai 200443, People's Republic of China
- ¹⁰ G.I. Budker Institute of Nuclear Physics SB RAS (BINP), Novosibirsk 630090, Russia
- ¹¹ GSI Helmholtzcentre for Heavy Ion Research GmbH, D-64291 Darmstadt, Germany
- ¹² Guangxi Normal University, Guilin 541004, People's Republic of China
- ¹³ Guangxi University, Nanning 530004, People's Republic of China
- ¹⁴ Hangzhou Normal University, Hangzhou 310036, People's Republic of China
- ¹⁵ Helmholtz Institute Mainz, Johann-Joachim-Becher-Weg 45, D-55099 Mainz, Germany
- ¹⁶ Henan Normal University, Xinxiang 453007, People's Republic of China
- ¹⁷ Henan University of Science and Technology, Luoyang 471003, People's Republic of China
- ¹⁸ Huangshan College, Huangshan 245000, People's Republic of China
- ¹⁹ Hunan Normal University, Changsha 410081, People's Republic of China
- ²⁰ Hunan University, Changsha 410082, People's Republic of China
- ²¹ Indian Institute of Technology Madras, Chennai 600036, India
- ²² Indiana University, Bloomington, Indiana 47405, USA
- ²³ INFN Laboratori Nazionali di Frascati , (A)INFN Laboratori Nazionali di Frascati, I-00044, Frascati, Italy; (B)INFN Sezione di Perugia, I-06100, Perugia, Italy; (C)University of Perugia, I-06100, Perugia, Italy
- ²⁴ INFN Sezione di Ferrara, INFN Sezione di Ferrara, I-44122, Ferrara, Italy
- ²⁵ Institute of Modern Physics, Lanzhou 730000, People's Republic of China
- ²⁶ Institute of Physics and Technology, Peace Ave. 54B, Ulaanbaatar 13330, Mongolia
- ²⁷ Jilin University, Changchun 130012, People's Republic of China
- ²⁸ Johannes Gutenberg University of Mainz, Johann-Joachim-Becher-Weg 45, D-55099 Mainz, Germany
- ²⁹ Joint Institute for Nuclear Research, 141980 Dubna, Moscow region, Russia
- ³⁰ Justus-Liebig-Universitaet Giessen, II. Physikalisches Institut, Heinrich-Buff-Ring 16, D-35392 Giessen, Germany
- ³¹ KVI-CART, University of Groningen, NL-9747 AA Groningen, The Netherlands
- ³² Lanzhou University, Lanzhou 730000, People's Republic of China
- ³³ Liaoning Normal University, Dalian 116029, People's Republic of China
- ³⁴ Liaoning University, Shenyang 110036, People's Republic of China
- ³⁵ Nanjing Normal University, Nanjing 210023, People's Republic of China
- ³⁶ Nanjing University, Nanjing 210093, People's Republic of China
- ³⁷ Nankai University, Tianjin 300071, People's Republic of China
- ³⁸ North China Electric Power University, Beijing 102206, People's Republic of China
- ³⁹ Peking University, Beijing 100871, People's Republic of China
- ⁴⁰ Qufu Normal University, Qufu 273165, People's Republic of China
- ⁴¹ Shandong Normal University, Jinan 250014, People's Republic of China
- ⁴² Shandong University, Jinan 250100, People's Republic of China
- ⁴³ Shanghai Jiao Tong University, Shanghai 200240, People's Republic of China
- ⁴⁴ Shanxi Normal University, Linfen 041004, People's Republic of China
- ⁴⁵ Shanxi University, Taiyuan 030006, People's Republic of China
- ⁴⁶ Sichuan University, Chengdu 610064, People's Republic of China
- ⁴⁷ Soochow University, Suzhou 215006, People's Republic of China
- ⁴⁸ South China Normal University, Guangzhou 510006, People's Republic of China
- ⁴⁹ Southeast University, Nanjing 211100, People's Republic of China
- ⁵⁰ State Key Laboratory of Particle Detection and Electronics, Beijing 100049, Hefei 230026, People's Republic of China
- ⁵¹ Sun Yat-Sen University, Guangzhou 510275, People's Republic of China
- ⁵² Suranaree University of Technology, University Avenue 111, Nakhon Ratchasima 30000, Thailand
- ⁵³ Tsinghua University, Beijing 100084, People's Republic of China
- ⁵⁴ Turkish Accelerator Center Particle Factory Group, (A)Istanbul Bilgi University, 34060 Eyup, Istanbul, Turkey; (B)Near East University, Nicosia, North Cyprus, Mersin 10, Turkey
- ⁵⁵ University of Chinese Academy of Sciences, Beijing 100049, People's Republic of China
- ⁵⁶ University of Hawaii, Honolulu, Hawaii 96822, USA
- ⁵⁷ University of Jinan, Jinan 250022, People's Republic of China
- ⁵⁸ University of Manchester, Oxford Road, Manchester, M13 9PL, United Kingdom
- ⁵⁹ University of Minnesota, Minneapolis, Minnesota 55455, USA
- ⁶⁰ University of Muenster, Wilhelm-Klemm-Str. 9, 48149 Muenster, Germany

⁶¹ *University of Oxford, Keble Rd, Oxford, UK OX13RH*

⁶² *University of Science and Technology Liaoning, Anshan 114051, People's Republic of China*

⁶³ *University of Science and Technology of China, Hefei 230026, People's Republic of China*

⁶⁴ *University of South China, Hengyang 421001, People's Republic of China*

⁶⁵ *University of the Punjab, Lahore-54590, Pakistan*

⁶⁶ *University of Turin and INFN, INFN, I-10125, Turin, Italy*

⁶⁷ *Uppsala University, Box 516, SE-75120 Uppsala, Sweden*

⁶⁸ *Wuhan University, Wuhan 430072, People's Republic of China*

⁶⁹ *Xinyang Normal University, Xinyang 464000, People's Republic of China*

⁷⁰ *Zhejiang University, Hangzhou 310027, People's Republic of China*

⁷¹ *Zhengzhou University, Zhengzhou 450001, People's Republic of China*

^a *Also at Bogazici University, 34342 Istanbul, Turkey*

^b *Also at the Moscow Institute of Physics and Technology, Moscow 141700, Russia*

^c *Also at the Novosibirsk State University, Novosibirsk, 630090, Russia*

^d *Also at the NRC "Kurchatov Institute", PNPI, 188300, Gatchina, Russia*

^e *Also at Istanbul Arel University, 34295 Istanbul, Turkey*

^f *Also at Goethe University Frankfurt, 60323 Frankfurt am Main, Germany*

^g *Also at Key Laboratory for Particle Physics, Astrophysics and Cosmology, Ministry of Education; Shanghai Key Laboratory for Particle Physics and Cosmology; Institute of Nuclear and Particle Physics, Shanghai 200240, People's Republic of China*

^h *Also at Key Laboratory of Nuclear Physics and Ion-beam Application (MOE) and Institute of Modern Physics, Fudan University, Shanghai 200443, People's Republic of China*

ⁱ *Also at Harvard University, Department of Physics, Cambridge, MA, 02138, USA*

^j *Currently at: Institute of Physics and Technology, Peace Ave.54B, Ulaanbaatar 13330, Mongolia*

^k *Also at State Key Laboratory of Nuclear Physics and Technology, Peking University, Beijing 100871, People's Republic of China*

^l *School of Physics and Electronics, Hunan University, Changsha 410082, China*

^m *Also at Guangdong Provincial Key Laboratory of Nuclear Science, Institute of Quantum Matter, South China Normal University, Guangzhou 510006, China*

ⁿ *Frontiers Science Center for Rare Isotopes, Lanzhou University, Lanzhou 730000, People's Republic of China*

^o *Lanzhou Center for Theoretical Physics, Lanzhou University, Lanzhou 730000, People's Republic of China*

(Dated: **March 15, 2021**)

We report a study of the processes $e^+e^- \rightarrow K^+D_s^-D^{*0}$ and $K^+D_s^{*-}D^0$ based on e^+e^- annihilation samples collected with the BESIII detector operating at BEPCII at five center-of-mass energies ranging from 4.628 to 4.698 GeV with a total integrated luminosity of 3.7 fb^{-1} . An excess of events over the known contributions of the conventional charmed mesons is observed near the $D_s^-D^{*0}$ and $D_s^{*-}D^0$ mass thresholds in the K^+ recoil-mass spectrum for events collected at $\sqrt{s} = 4.681 \text{ GeV}$. The structure matches a mass-dependent-width Breit-Wigner line shape, whose pole mass and width are determined as $(3982.5_{-2.6}^{+1.8} \pm 2.1) \text{ MeV}/c^2$ and $(12.8_{-4.4}^{+5.3} \pm 3.0) \text{ MeV}$, respectively. The first uncertainties are statistical and the second are systematic. The significance of the resonance hypothesis is estimated to be 5.3σ over the contributions only from the conventional charmed mesons. This is the first candidate for a charged hidden-charm tetraquark with strangeness, decaying into $D_s^-D^{*0}$ and $D_s^{*-}D^0$. However, the properties of the excess need further exploration with more statistics.

Recent observations of nonstrange hidden-charm tetraquark candidates with quark content $c\bar{c}q\bar{q}'$ ($q^{(\prime)} = u$ or d), referred to as the Z_c states, have opened a new chapter in hadron spectroscopy [1–6]. In electron-positron annihilation, in particular, both the charged and neutral $Z_c(3900)$ and $Z_c(4020)$ have been observed at the BESIII, Belle, and CLEO experiments in a variety of decay modes [7–16]. Assuming SU(3) flavor symmetry, one would expect the existence of strange partners to the Z_c , denoted as Z_{cs} , with quark content $c\bar{c}s\bar{q}$ [17]. No experimental searches for Z_{cs} states have yet been reported.

The existence of a Z_{cs} state with a mass lying around the $D_s^-D^{*0}$ and $D_s^{*-}D^0$ thresholds has been predicted in several theoretical models, including tetraquark scenarios [18, 19], the $D_s\bar{D}^*$ molecular model [20, 21], the hadro-quarkonium model [19], and in the initial-single-chiral-particle-emission mechanism [22]. Like the

Z_c states, the decay rate of the Z_{cs} to open-charm final states is expected to be larger than the decay rate to charmonium final states [5]. Hence, one promising method to search for the Z_{cs} state is through its decays to $D_s^-D^{*0}$ and $D_s^{*-}D^0$.

In this Letter, we report on a study of the process $e^+e^- \rightarrow K^+D_s^-D^{*0}$ and $K^+D_s^{*-}D^0$ [$e^+e^- \rightarrow K^+(D_s^-D^{*0} + D_s^{*-}D^0)$ for short] at center-of-mass energies $\sqrt{s} = 4.628, 4.641, 4.661, 4.681, \text{ and } 4.698 \text{ GeV}$. The data samples have a total integrated luminosity of 3.7 fb^{-1} and were accumulated by the BESIII detector at the BEPCII collider. Details about BEPCII and BESIII can be found in Refs. [23–25]. To improve the signal-selection efficiency, a partial-reconstruction technique is implemented in which only the charged K^+ (the *bachelor* K^+) and the D_s^- are reconstructed. Here and elsewhere, charge-conjugate modes are always implied, unless ex-

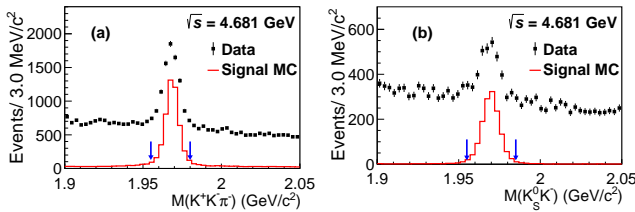


FIG. 1. Distributions of the invariant mass $M(K^+K^-\pi^-)$ (a) and $M(K_S^0K^-)$ (b) in data and MC simulations at $\sqrt{s} = 4.681$ GeV. The $Z_{cs}(3985)^-$ signal MC component is normalized to the observed D_s^- yield in data. Arrows indicate the mass region requirements.

explicitly stated otherwise. To improve the signal purity, we only reconstruct the decays $D_s^- \rightarrow K^+K^-\pi^-$ and $K_S^0K^-$, which have large branching fractions (BFs). By reconstructing the D_s^- meson, the flavors of the missing D^0 and the bachelor K^+ are fixed. We observe an enhancement near the $D_s^-D^{*0}$ and $D_s^{*-}D^0$ mass thresholds in the K^+ recoil-mass spectrum for events collected at $\sqrt{s} = 4.681$ GeV and carry out a fit to the enhancement with a possible new Z_{cs} candidate, denoted as $Z_{cs}(3985)^-$, in the K^+ recoil-mass spectra at different energy points.

Monte Carlo (MC) simulation samples are produced under a GEANT4-based [26] framework, as detailed in Ref. [27]. For the three-body nonresonant (NR) signal process, $e^+e^- \rightarrow K^+(D_s^-D^{*0} + D_s^{*-}D^0)$, the final-state particles are simulated assuming nonresonant production [27]. For the simulation of the $Z_{cs}(3985)^-$ signal process, $e^+e^- \rightarrow K^+Z_{cs}(3985)^-$, we let the $Z_{cs}(3985)^-$ decay into the $D_s^-D^{*0}$ and $D_s^{*-}D^0$ final states with equal rates. The $Z_{cs}(3985)^-$ state is assigned a spin parity of 1^+ , as the corresponding production and subsequent decay processes are both in the most favored S wave. However, other spin-parity assignments are allowed, and these are tested as systematic variations.

To identify the processes $e^+e^- \rightarrow K^+(D_s^-D^{*0} + D_s^{*-}D^0)$, we reconstruct combinations of the bachelor K^+ and the decays $D_s^- \rightarrow K^+K^-\pi^-$ or $K_S^0K^-$. Data taken at all five center-of-mass energy points are analyzed using the same procedure, but two-thirds of the data set at $\sqrt{s} = 4.681$ GeV was kept blinded until after the analysis strategy was established and validated [28]. We select events with at least four charged tracks and reconstruct the final states of K^\pm, π^\pm and $K_S^0 \rightarrow \pi^+\pi^-$ following the criteria in Ref. [29]. For the candidate of K_S^0 , we require its invariant mass within $0.485 < M(\pi^+\pi^-) < 0.511$ GeV/ c^2 . For the decay $D_s^- \rightarrow K^+K^-\pi^-$, to improve the signal purity, we only retain the D_s^- candidates within the Dalitz plot regions consistent with $D_s^- \rightarrow \phi\pi^-$ or $D_s^- \rightarrow K^*(892)^0K^-$ decays by requiring that the invariant masses satisfy either $M(K^+K^-) < 1.05$ GeV/ c^2 or $0.850 < M(K^+\pi^-) < 0.930$ GeV/ c^2 .

Figure 1 shows the $K^+K^-\pi^-$ and $K_S^0K^-$ invariant mass distributions for events at $\sqrt{s} = 4.681$ GeV, in which D_s^- peaks are clearly evident.

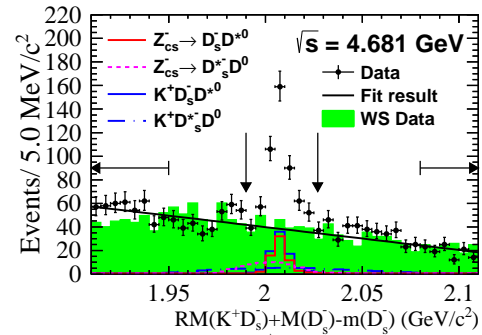


FIG. 2. Distribution of the $K^+D_s^-$ recoil mass in data and signal MC samples at $\sqrt{s} = 4.681$ GeV. Horizontal arrows indicate the sidebands and vertical arrows indicate the signal region. The magnitudes of the three-body nonresonant processes and $Z_{cs}(3985)^-$ signal processes are scaled arbitrarily. The histogram of wrong-sign (WS) events is scaled by a factor of 1.18 to match the sideband data.

All combinations with invariant mass in the region $1.955 < M(K^+K^-\pi^-) < 1.980$ GeV/ c^2 and $1.955 < M(K_S^0K^-) < 1.985$ GeV/ c^2 are identified as D_s^- meson candidates. Figure 2 shows the $K^+D_s^-$ recoil-mass spectrum for D_s^- candidate events at $\sqrt{s} = 4.681$ GeV, calculated using $RM(K^+D_s^-) + M(D_s^-) - m(D_s^-)$. Here, $RM(X) = ||p_{e^+e^-} - p_X||$, where $p_{e^+e^-}$ is the four-momentum of the initial e^+e^- system and p_X is the four-momentum of the system X , $M(D_s^-)$ is the reconstructed D_s^- mass, and $m(D_s^-)$ is the mass of the D_s^- reported by the PDG [30]. The variable $RM(K^+D_s^-) + M(D_s^-) - m(D_s^-)$ provides improved resolution compared to $RM(K^+D_s^-)$ [10]. A clear peak is seen in this distribution at the nominal D^{*0} mass, which corresponds to the final state $K^+D_s^-D^{*0}$. There is also a contribution from $K^+D_s^{*-}D^0$, which appears as a broader structure beneath the $K^+D_s^-D^{*0}$ signal. Therefore, we require $RM(K^+D_s^-) + M(D_s^-) - m(D_s^-)$ to be in the interval (1.990, 2.027) GeV/ c^2 to isolate the signal candidates of both signal processes.

To estimate the shape of combinatorial background, we use wrong-sign (WS) combinations of D_s^- and K^- candidates, rather than the right-sign D_s^- and K^+ candidates. The WS $K^-D_s^-$ recoil-mass distribution, scaled by a factor of 1.18, agrees with the data distribution in the sideband regions, (1.91, 1.95) GeV/ c^2 and (2.08, 2.11) GeV/ c^2 , as shown in Fig. 2. The number of background events within the signal region is estimated to be 282.6 ± 12.0 by a fit to the sideband data with a linear function, whose slope is determined from the WS data. In addition, the WS events are used to represent the combinatorial-background distribution of the recoil mass of the bachelor K^+ . This technique has been used previously in the observation of the $Z_c(4025)^+$ at BESIII [10]. We validate the use of the WS data-driven background modeling of both the $RM(K^+D_s^-)$ and $RM(K^+)$ spectra by comparing the corresponding distributions between WS combinations and background-only contributions. Furthermore, the $RM(K^+)$ distribution of the events in the sideband regions in Fig. 2 agrees well with that of the corresponding WS data.

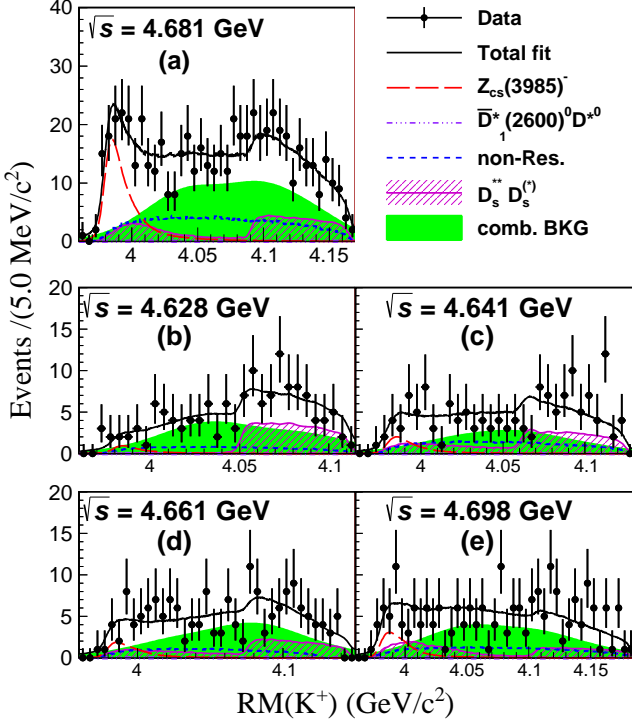


FIG. 3. Simultaneous unbinned maximum likelihood fit to the K^+ recoil-mass spectra in data at $\sqrt{s}=4.628, 4.641, 4.661, 4.681$ and 4.698 GeV. Note that the size of the $D^{*0}\bar{D}_1^*(2600)^0(\rightarrow D_s^- K^+)$ component is consistent with zero.

Figure 3(a) shows the $RM(K^+)$ distribution for events at $\sqrt{s} = 4.681$ GeV; an enhancement is evident in the region $RM(K^+) < 4$ GeV/ c^2 compared to the expectation from the WS events. This is clearly illustrated in the $RM(K^+)$ distribution in data with subtraction of the WS component in Fig. 4. The enhancement cannot be attributed to the NR signal processes $e^+e^- \rightarrow K^+(D_s^- D^{*0} + D_s^{*-} D^0)$. To understand potential contributions from the processes $e^+e^- \rightarrow D_s^{(*)-} D_s^{*+}(\rightarrow D^{(*)0} K^+)$ or $D^{(*)0} \bar{D}^{*0}(\rightarrow D_s^{(*)-} K^+)$, we examine all known $D_{(s)}^{*+}$ excited states [30, 31] using MC simulation samples. Dedicated exclusive MC studies show that none of these processes, including possible interference effects, exhibit a narrow structure below 4.0 GeV/ c^2 [28].

The following three processes that contain excited D_s^{*+} background have potential contributions to the $RM(K^+)$ spectrum: (1) $D_s^- D_{s1}^*(2536)^+(\rightarrow D^{*0} K^+)$, (2) $D_s^- D_{s2}^*(2573)^+(\rightarrow D^0 K^+)$, and (3) $D_s^- D_{s1}^*(2700)^+(\rightarrow D^{*0} K^+)$. We estimate their production cross sections by studying several control samples. The yields for channel (1) are estimated by analyzing the $D_{s1}^*(2536)^+$ peak in the $D^{*0} K^+$ mass spectra using two separate partially reconstructed samples: $K^+ D_s^-$ (with D^{*0} missing) and $K^+ D^{*0}$ (with D_s^- missing). For channel (2), control samples are selected by reconstructing $D^0 K^+ \gamma$ (with missing D_s^-) or $K^+ D_s^{*-}$

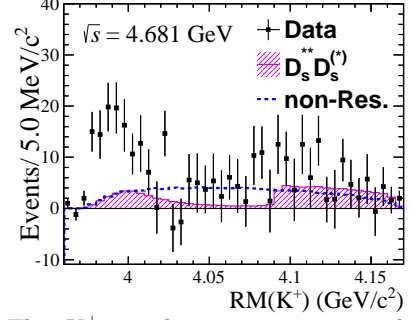


FIG. 4. The K^+ recoil-mass spectrum in data at $\sqrt{s} = 4.681$ GeV after subtraction of the combinatorial backgrounds.

(with missing D^0). The $D_{s2}^*(2573)^+$ yield is obtained from combined fits to the $D^0 K^+$ mass spectra. From this, the contribution from channel (2) to the signal candidates in Fig. 3 is evaluated. For channel (3), a control sample of $e^+e^- \rightarrow D_s^- D_{s1}^*(2700)^+(\rightarrow D^0 K^+)$ is selected by detecting the $D_s^- K^+$ recoiling against a missing D^0 . We then use the BF ratio of $\mathcal{B}(D_{s1}^*(2700)^+ \rightarrow D^{*0} K^+)/\mathcal{B}(D_{s1}^*(2700)^+ \rightarrow D^0 K^+) = 0.91 \pm 0.18$ [32] to estimate the strength of this background contribution. The shapes in $RM(K^+)$ of these three channels are extracted from MC samples, whereas the normalization is derived from the control samples. The estimated background contributions of the channels (1), (2) and (3) in the $RM(K^+)$ spectrum at $\sqrt{s} = 4.681$ GeV are $54.4 \pm 8.0, 19.1 \pm 7.6$ and 15.0 ± 13.3 events, respectively. For the other energy points, the estimated yields of the three channels are given in Ref. [28].

Two processes with excited nonstrange \bar{D}^{*0} states that produce potential enhancements around 4 GeV/ c^2 in $RM(K^+)$ are $D^{*0} \bar{D}_1^*(2600)^0(\rightarrow D_s^- K^+)$ [30, 31] and $D^0 \bar{D}_3^*(2750)^0(\rightarrow D_s^{*-} K^+)$. In these processes, the $RM(K^+)$ spectrum is distorted due to limited production phase space. The first process is studied using an amplitude analysis of the control sample $e^+e^- \rightarrow D^{*0} \bar{D}_1^*(2600)^0(\rightarrow D^- \pi^+)$ at all five energy points. Since the ratio $\mathcal{B}(\bar{D}_1^*(2600)^0 \rightarrow D_s^- K^+)/\mathcal{B}(\bar{D}_1^*(2600)^0 \rightarrow D^- \pi^+)$ is unknown, it is difficult to project the results of the amplitude analysis into our signal channel. Instead, we determine the ratio in our nominal fit, providing a constraint on the size of the $D^{*0} \bar{D}_1^*(2600)^0(\rightarrow D_s^- K^+)$ component at the different energy points. For the second process, no significant signal is observed in the control sample $e^+e^- \rightarrow D^0 \bar{D}_3^*(2750)^0(\rightarrow D^- \pi^+)$. Assuming the relative BF ratio $\mathcal{B}(D_3^* \rightarrow D_s^{*-} K^+)/\mathcal{B}(D_3^* \rightarrow D^- \pi^+) = 4.1\%$ [33], the contribution of the $D^0 \bar{D}_3^*(2750)^0$ channel to Fig. 3 is estimated to be 0.0 ± 0.4 events, and the corresponding upper limit is taken into account as a source of systematic uncertainty.

As no known processes explain the observed enhancement in the $RM(K^+)$ spectrum, which is very close to the threshold of $D_s^- D^{*0}$ (3975.2 MeV/ c^2) and $D_s^{*-} D^0$ (3977.0 MeV/ c^2), we consider the possibility of describing the structure as a $D_s^- D^{*0}$ and $D_s^{*-} D^0$ resonance with a mass-dependent-width Breit-Wigner line

shape, denoted as $Z_{cs}(3985)^-$. A simultaneous unbinned maximum likelihood fit is performed to the $RM(K^+)$ spectra at all five energy points, as shown in Fig. 3. The $Z_{cs}(3985)^-$ component is modeled by the product of an S -wave Breit-Wigner shape with a mass-dependent width of the following form

$$\mathcal{F}_j(M) \propto \left| \frac{\sqrt{q \cdot p_j}}{M^2 - m_0^2 + im_0(f\Gamma_1(M) + (1-f)\Gamma_2(M))} \right|^2,$$

where $\Gamma_j(M) = \Gamma_0 \cdot \frac{p_j}{p_j^*} \cdot \frac{m_0}{M}$ with subscript $j = 1$ and $j = 2$ standing for the decays of $Z_{cs}(3985)^- \rightarrow D_s^- D^{*0}$ and $Z_{cs}(3985)^- \rightarrow D_s^{*-} D^0$, respectively. Here, M is the reconstructed mass; m_0 is the resonance mass; Γ_0 is the width; q is the K^+ momentum in the initial e^+e^- system; p_1 (p_2) is the D_s^- (D_s^{*-}) momentum in the rest frame of the $D_s^- D^{*0}$ ($D_s^{*-} D^0$) system; p_1^* (p_2^*) is the D_s^- (D_s^{*-}) momentum in the rest frame of the $D_s^- D^{*0}$ ($D_s^{*-} D^0$) system at $M=m_0$. We define $f = [\mathcal{B}_1/(\mathcal{B}_1 + \mathcal{B}_2)]$, where \mathcal{B}_j is the BF of the j th decay. We assume $f = 0.5$ in the nominal fit and take variations of f into account in the studies of systematic uncertainty.

The $Z_{cs}(3985)^-$ signal shape, which is used in the fit depicted in Fig. 3, is the f -dependent sum of the efficiency-weighted \mathcal{F}_j functions convolved with a resolution function, which is obtained from MC simulation. The resolution is about $5 \text{ MeV}/c^2$ and is asymmetric due to the contribution from ISR. The parametrization of the combinatorial-background shape is derived from the kernel estimate [34] of the WS distribution, whose normalization is fixed to the number of the fitted background events within the decorrelated $RM(K^+ D_s^-)$ signal window. The shapes of the NR and $D^{*0} \bar{D}_1^*(2600)^0 (\rightarrow D_s^- K^+)$ signals are taken from the MC simulation. The size of the NR component at each energy point and the ratio $\mathcal{B}(\bar{D}_1^*(2600)^0 \rightarrow D_s^- K^+)/\mathcal{B}(\bar{D}_1^*(2600)^0 \rightarrow D^- \pi^+)$ are free parameters in the fit. In addition, a component that describes the total contributions of the excited D_s^{**+} processes is included, whose shape is taken from MC simulation and its size is fixed according to the yields estimated from the control-sample studies.

From the fit, the parameters m_0 and Γ_0 are determined to be $(3985.2_{-2.0}^{+2.1}) \text{ MeV}/c^2$ and $(13.8_{-5.2}^{+8.1}) \text{ MeV}$, respectively. The significance of the signal is calculated taking into account the look-elsewhere effect [35], where 5000 pseudodatasets are produced with the sum of null- $Z_{cs}(3985)^-$ models and fitted with the same strategy as the nominal fit to obtain the distribution of $-2 \ln(L_0/L_{\max})$, where L_0 and L_{\max} are fitted likelihood values under the null- $Z_{cs}(3985)^-$ hypothesis and alternative hypothesis, respectively. In the generation of the pseudodata, the systematic uncertainties relevant to determine the signal yields, as marked in Table II in Ref. [28] are considered. The resulting distribution is found to be well described by a χ^2 distribution with 13.8 degrees of freedom. With an observed value of $-2 \ln(L_0/L_{\max}) = 59.14$, we obtain a significance of 5.3σ . The number of $Z_{cs}(3985)^-$ events observed at $\sqrt{s} = 4.681 \text{ GeV}$ is the most prominent compared to

TABLE I. The results for the cross section measurement at each energy point. The upper limits in the parenthesis correspond to 90% confidence level after considering the systematic uncertainties.

\sqrt{s} (GeV)	\mathcal{L}_{int} (pb^{-1})	n_{sig}	$f_{\text{corr}} \bar{\epsilon}$ (%)	$\sigma^B \cdot \mathcal{B}$ (pb)
4.628	511.1	$4.2_{-4.2}^{+6.1}$	1.03	$0.8_{-0.8}^{+1.2} \pm 0.6 (< 3.0)$
4.641	541.4	$9.3_{-6.2}^{+7.3}$	1.09	$1.6_{-1.1}^{+1.2} \pm 1.3 (< 4.4)$
4.661	523.6	$10.6_{-7.4}^{+8.9}$	1.28	$1.6_{-1.1}^{+1.3} \pm 0.8 (< 4.0)$
4.681	1643.4	$85.2_{-15.6}^{+17.6}$	1.18	$4.4_{-0.8}^{+0.9} \pm 1.4$
4.698	526.2	$17.8_{-7.2}^{+8.1}$	1.42	$2.4_{-1.0}^{+1.1} \pm 1.2 (< 4.7)$

TABLE II. Summary of systematic uncertainties on the $Z_{cs}(3985)^-$ resonance parameters. The total systematic uncertainty corresponds to a quadrature sum of all individual items. The global signal significance after taking into account the systematic item marked with * is listed.

Source	Mass (MeV/c^2)	Width (MeV)	Significance
Mass scale	0.5		
Resolution*	0.2	1.0	5.7σ
f factor*	0.2	1.0	5.6σ
Signal model*	1.0	2.6	5.7σ
Backgrounds*	0.5	0.5	5.6σ
Efficiencies	0.1	0.2	
D_s^{**} states*	1.0	3.4	5.4σ
$\sigma^B [K^+ Z_{cs}(3985)^-]$	0.6	1.7	
Total	1.7	4.9	

the other four energy points. If we fit only to data at $\sqrt{s} = 4.681 \text{ GeV}$, we obtain consistent $Z_{cs}(3985)^-$ resonance parameters.

The Born cross section $\sigma^B[e^+e^- \rightarrow K^+ Z_{cs}(3985)^- + \text{c.c.}]$ times the sum of BFs of the decays $Z_{cs}(3985)^- \rightarrow D_s^- D^{*0} + D_s^{*-} D^0$ is equal to $\frac{n_{\text{sig}}}{\mathcal{L}_{\text{int}} f_{\text{corr}} \bar{\epsilon}}$, where n_{sig} is the number of the observed signal events, \mathcal{L}_{int} is the integrated luminosity, and $\bar{\epsilon}$ is the BF-weighted detection efficiency. We define $f_{\text{corr}} \equiv (1 + \delta_{\text{ISR}}) \frac{1}{|1 - \Pi|^2}$, where $(1 + \delta_{\text{ISR}})$ is the radiative-correction factor and $\frac{1}{|1 - \Pi|^2}$ is the vacuum-polarization factor [36]. The numerical results are listed in Table I.

Sources of systematic uncertainties on the measurement of the $Z_{cs}(3985)^-$ resonance parameters and the cross section are studied, as explained in Ref. [28]. The main sources include the mass scaling, detector resolution, the signal model, background models and the input cross section line shape for $\sigma^B[e^+e^- \rightarrow K^+ Z_{cs}(3985)^-]$. The contributions to the systematic uncertainties on the resonance parameters and cross sections are given in Table II and Ref. [28], respectively. In addition, the global signal significances after taking into account the look-elsewhere effect under different systematic effects are listed in Table II.

In summary, we study the reactions $e^+e^- \rightarrow K^+(D_s^- D^{*0} + D_s^{*-} D^0)$ based on 3.7 fb^{-1} of data collected at $\sqrt{s} = 4.628, 4.641, 4.661, 4.681, \text{ and } 4.698 \text{ GeV}$, and observe an enhancement near the $D_s^- D^{*0}$ and $D_s^{*-} D^0$

mass thresholds in the K^+ recoil-mass spectrum for events collected at $\sqrt{s} = 4.681$ GeV. While the known charmed mesons cannot explain the excess, it matches a hypothesis of a $D_s^- D^{*0}$ and $D_s^{*-} D^0$ resonant structure $Z_{cs}(3985)^-$ with a mass-dependent-width Breit-Wigner line shape well; a fit gives the resonance mass of $(3985.2_{-2.0}^{+2.1} \pm 1.7)$ MeV/ c^2 and width of $(13.8_{-5.2}^{+8.1} \pm 4.9)$ MeV. This corresponds to a pole position $m_{\text{pole}} - i\frac{\Gamma_{\text{pole}}}{2}$ of

$$m_{\text{pole}}[Z_{cs}(3985)^-] = (3982.5_{-2.6}^{+1.8} \pm 2.1) \text{ MeV}/c^2,$$

$$\Gamma_{\text{pole}}[Z_{cs}(3985)^-] = (12.8_{-4.4}^{+5.3} \pm 3.0) \text{ MeV}.$$

The first uncertainties are statistical and the second are systematic. The significance of this resonance hypothesis is estimated to be 5.3σ over the pure contributions from the conventional charmed mesons. The $Z_{cs}(3985)^-$ candidate reported here would couple to at least one of $D_s^- D^{*0}$ and $D_s^{*-} D^0$, and has unit charge, the quark composition is most likely $c\bar{c}s\bar{u}$. Hence, it would become the first Z_{cs} tetraquark candidate observed. The measured mass is close to the mass threshold of $D_s\bar{D}^*$ and $D_s^*\bar{D}$, which is consistent with the theoretical calculations in Ref. [18, 20–22]. In addition, the Born cross sections $\sigma^B[e^+e^- \rightarrow K^+ Z_{cs}(3985)^- + \text{c.c.}]$ times the sum of the branching fractions for $Z_{cs}(3985)^- \rightarrow D_s^- D^{*0} + D_s^{*-} D^0$ decays are measured at the five energy points. Because of the limited size of the statistics, only a one-dimensional fit is implemented and the potential interference effects are neglected. As shown in Figs. 5 and 6 of Ref. [28], we find no evidence for enhancements due to interference below 4 GeV/ c^2 . Even so, the properties of the observed excess might not be fully explored and there exist other possibilities of explaining the near-threshold

enhancement. To further improve studies of the excess, more statistics are necessary in order to carry out an amplitude analysis.

The BESIII Collaboration thanks the staff of BEPCII and the IHEP computing center for their strong support. This work is supported in part by National Key Basic Research Program of China under Contract Nos. 2015CB856700; National Key Research and Development Program of China under Nos. 2020YFA0406300, 2020YFA0406400; National Natural Science Foundation of China (NSFC) under Contracts Nos. 11625523, 11635010, 11735014, 11805086, 11822506, 11835012, 11935015, 11935016, 11935018, 11961141012; the Chinese Academy of Sciences (CAS) Large-Scale Scientific Facility Program; the CAS PIFI program; Joint Large-Scale Scientific Facility Funds of the NSFC and CAS under Contracts Nos. U1732263, U1832207; CAS Key Research Program of Frontier Sciences under Contracts Nos. QYZDJ-SSW-SLH003, QYZDJ-SSW-SLH040; 100 Talents Program of CAS; the Fundamental Research Funds for the Central Universities; INPAC and Shanghai Key Laboratory for Particle Physics and Cosmology; ERC under Contract No. 758462; German Research Foundation DFG under Contracts Nos. 443159800, Collaborative Research Center CRC 1044, FOR 2359, GRK 2149; Istituto Nazionale di Fisica Nucleare, Italy; Ministry of Development of Turkey under Contract No. DPT2006K-120470; National Science and Technology fund; Olle Engkvist Foundation under Contract No. 200-0605; STFC (United Kingdom); The Knut and Alice Wallenberg Foundation (Sweden) under Contract No. 2016.0157; The Royal Society, UK under Contracts Nos. DH140054, DH160214; The Swedish Research Council; U. S. Department of Energy under Contracts Nos. DE-FG02-05ER41374, DE-SC-0012069.

-
- [1] N. Brambilla, S. Eidelman, C. Hanhart *et al.*, Phys. Rep. **873**, 1 (2020).
- [2] F. K. Guo, C. Hanhart, U. G. Meißner, Q. Wang, Q. Zhao and B. S. Zou, Rev. Mod. Phys. **90**, 015004 (2018).
- [3] H. X. Chen, W. Chen, X. Liu and S. L. Zhu, Phys. Rep. **639**, 1 (2016).
- [4] N. Brambilla *et al.*, Eur. Phys. J. C **71**, 1534 (2011).
- [5] S. L. Olsen, T. Skwarnicki and D. Zieminska, Rev. Mod. Phys. **90**, 015003 (2018).
- [6] S. L. Olsen, Front. Phys. (Beijing) **10**, 121-154 (2015).
- [7] M. Ablikim *et al.* (BESIII Collaboration), Phys. Rev. Lett. **110**, 252001 (2013).
- [8] M. Ablikim *et al.* (BESIII Collaboration), Phys. Rev. Lett. **111**, 242001 (2013).
- [9] M. Ablikim *et al.* (BESIII Collaboration), Phys. Rev. Lett. **112**, 022001 (2014).
- [10] M. Ablikim *et al.* (BESIII Collaboration), Phys. Rev. Lett. **112**, 132001 (2014).
- [11] M. Ablikim *et al.* (BESIII Collaboration), Phys. Rev. Lett. **113**, 212002 (2014).
- [12] M. Ablikim *et al.* (BESIII Collaboration), Phys. Rev. Lett. **115**, 112003 (2015).
- [13] M. Ablikim *et al.* (BESIII Collaboration), Phys. Rev. Lett. **115**, 182002 (2015).
- [14] M. Ablikim *et al.* (BESIII Collaboration), Phys. Rev. Lett. **115**, 222002 (2015).
- [15] Z. Q. Liu *et al.* (Belle Collaboration), Phys. Rev. Lett. **110**, 252002 (2013); Erratum: [Phys. Rev. Lett. **111**, 019901 (2013)].
- [16] T. Xiao, S. Dobbs, A. Tomaradze and K. K. Seth, Phys. Lett. B **727**, 366 (2013).
- [17] M. B. Voloshin, Phys. Lett. B **798**, 135022 (2019).
- [18] D. Ebert, R. N. Faustov and V. O. Galkin, Eur. Phys. J. C **58**, 399 (2008).
- [19] J. Ferretti and E. Santopinto, JHEP **04**, 119 (2020).
- [20] S. H. Lee, M. Nielsen and U. Wiedner, J. Korean Phys. Soc. **55**, 424 (2009).
- [21] J. M. Dias, X. Liu and M. Nielsen, Phys. Rev. D **88**, 096014 (2013).
- [22] D. Y. Chen, X. Liu and T. Matsuki, Phys. Rev. Lett. **110**, 232001 (2013).
- [23] M. Ablikim *et al.* (BESIII Collaboration), Nucl. Instrum.

- Meth. A **614**, 345 (2010).
- [24] C. H. Yu *et al.*, Proceedings of IPAC2016, Busan, Korea, 2016, doi:10.18429/JACoW-IPAC2016-TUYA01.
- [25] M. Ablikim *et al.* (BESIII Collaboration), Chin. Phys. C **44**, 040001 (2020).
- [26] S. Agostinelli *et al.* (GEANT4 Collaboration), Nucl. Instrum. Meth. A **506**, 250 (2003).
- [27] M. Ablikim *et al.* (BESIII Collaboration), Chin. Phys. C **43**, 031001 (2019).
- [28] See Supplemental Material for additional analysis information, which includes Ref. [30, 37].
- [29] M. Ablikim *et al.* (BESIII Collaboration), Phys. Rev. Lett. **122**, 071802 (2019).
- [30] P. A. Zyla *et al.* (Particle Data Group), Prog. Theor. Exp. Phys. **2020**, 083C01 (2020).
- [31] R. Aaij *et al.* (LHCb Collaboration), Phys. Rev. D **101**, 032005 (2020).
- [32] B. Aubert *et al.* (BaBar Collaboration), Phys. Rev. D **80**, 092003 (2009).
- [33] S. Godfrey and K. Moats, Phys. Rev. D **93**, 034035 (2016).
- [34] K. S. Cranmer, Comput. Phys. Commun. **136**, 198 (2001).
- [35] E. Gross and O. Vitells, Eur. Phys. J. C **70**, 525 (2010).
- [36] F. Jegerlehner, Nuovo Cim. C **034S1**, 31 (2011).
- [37] A. M. Badalian, L. P. Kok, M. I. Polikarpov and Y. A. Simonov, Phys. Rept. **82**, 31 (1982).

Supplemental Material for “Observation of a Near-Threshold Structure in the K^+ Recoil Mass Spectra in $e^+e^- \rightarrow K^+(D_s^-D^{*0} + D_s^{*-}D^0)$ ”

Appendix A: Additional information: studies of the excess in K^+ recoil-mass spectrum

Figure 1 shows the distribution of the $K^+D_s^-$ recoil-mass in data and MC simulation samples at $\sqrt{s} = 4.628, 4.641, 4.661$ and 4.698 GeV, after the same selection criteria as those imposed for the data shown in Fig. 2 of the main letter. Table I lists the estimated sizes of excited D_s^{*+} or \bar{D}^{*0} contributions at each energy point, quoted in the simultaneous fit. In addition, two-dimensional plots of $M(K^+D_s^-)$ versus $RM(K^+)$ in data for events in the signal region and WS events at $\sqrt{s} = 4.681$ GeV are shown in Fig. 2.

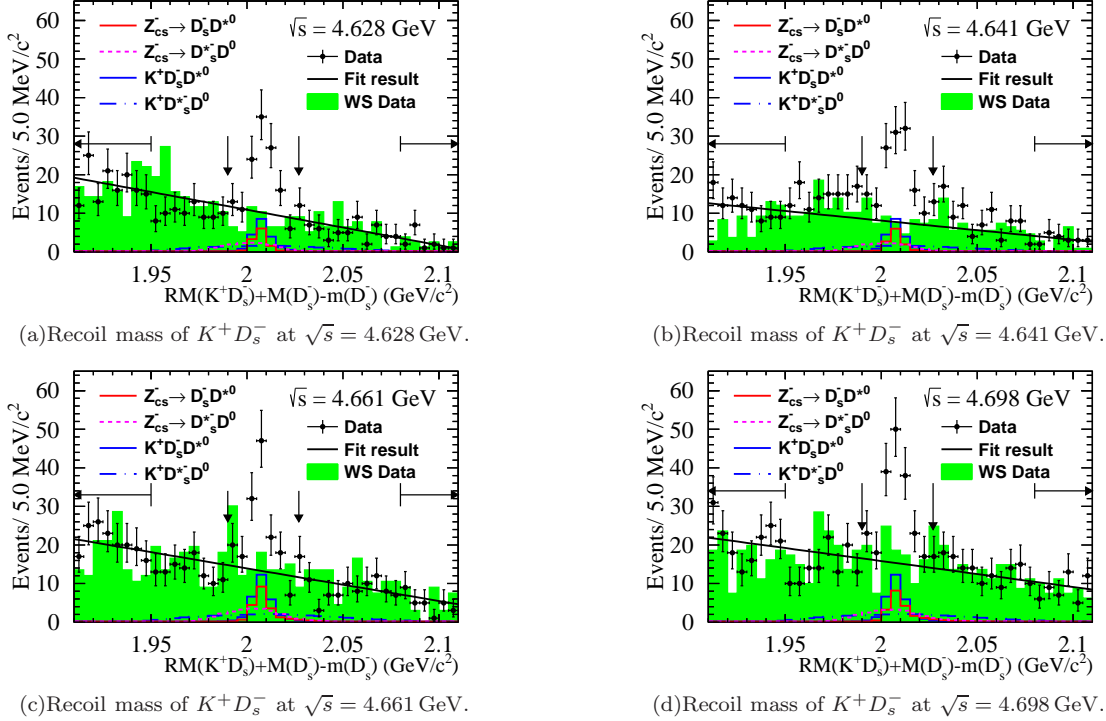


FIG. 1. Distribution of the $K^+D_s^-$ recoil-mass in data and signal MC samples at different center-of-mass energies. Definitions of plotted components are the same as those in Fig. 2 of the main paper.

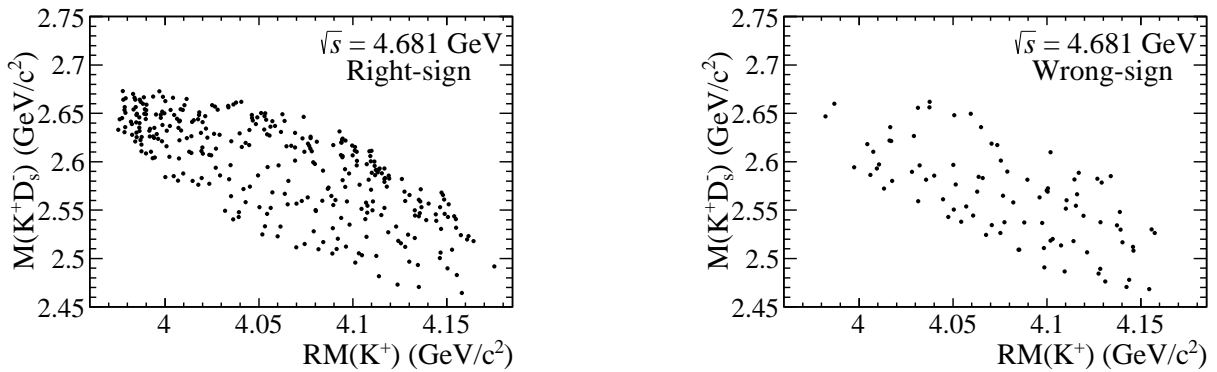


FIG. 2. Two-dimensional distributions of $M(K^+D_s^-)$ vs. $RM(K^+)$ for data in the signal region (left) and WS events (right) at $\sqrt{s} = 4.681$ GeV.

TABLE I. Summary of the estimated sizes of excited D_s^{**+} or \bar{D}^{**0} contributions at each energy point. “-” means the production is not allowed kinematically.

\sqrt{s} (GeV)	4.628	4.641	4.661	4.681	4.698
$D_{s1}(2536)^+(K^+D^{*0})D_s^-$	41.2 ± 6.3	26.2 ± 5.4	23.9 ± 5.6	54.4 ± 8.0	15.3 ± 4.2
$D_{s2}^*(2573)^+(K^+D^0)D_s^{*-}$	-	-	-	19.1 ± 7.6	17.3 ± 7.3
$D_{s1}^*(2700)^+(K^+D^{*0})D_s^-$	0.0 ± 1.8	18.6 ± 8.7	16.6 ± 7.8	15.0 ± 13.3	7.7 ± 8.4
$D_3^*(2750)^0(\rightarrow D_s^{*-}K^+)D^0$	0.0 ± 0.1	0.0 ± 0.2	0.0 ± 0.2	0.0 ± 0.4	0.0 ± 0.5

Appendix B: Exploration of potential $D_{(s)}^{**}$ backgrounds

To understand the potential backgrounds from excited $D_{(s)}^{**}$ states, all reported states in the PDG [30] whose production and decay is allowed within the available phase-space at $\sqrt{s} = 4.681$ GeV are investigated. The corresponding $RM(K^+)$ distributions of the MC simulations are plotted in Figs. 3 and 4. Furthermore, possible interferences among those excited $D_{(s)}^{**}$ states are systematically scanned, and the choices with the largest interferences around $RM(K^+) = 4.0$ GeV/ c^2 are compared with the distributions in data, shown in Fig. 5 and Fig. 6. It is evident that none of the states can explain the narrow peaking structure below 4.0 GeV/ c^2 .

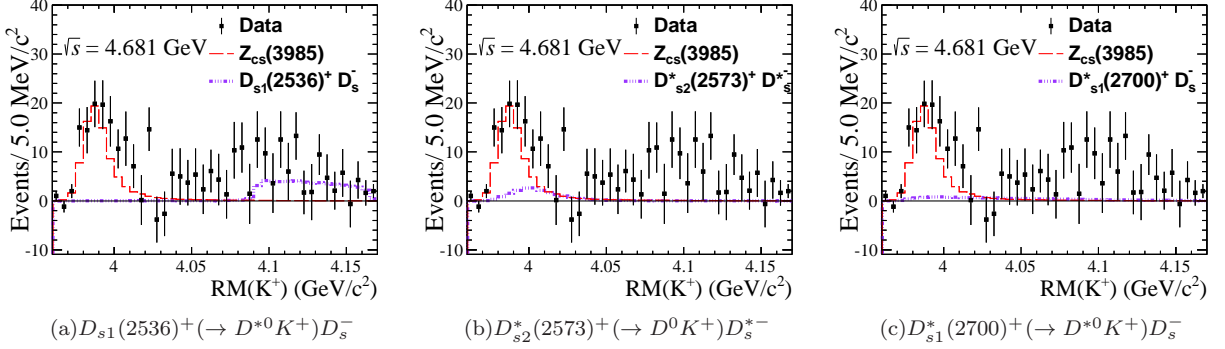


FIG. 3. K^+ recoil-mass spectra in data with the WS background contributions subtracted, and MC simulations of the excited D_s^{**} states in $e^+e^- \rightarrow D_s^{**+}D_s^{*-}$. The $Z_{cs}(3985)^-$ shapes are normalized to the yields observed in data and those of the D_s^{**} states are scaled according to the control samples.

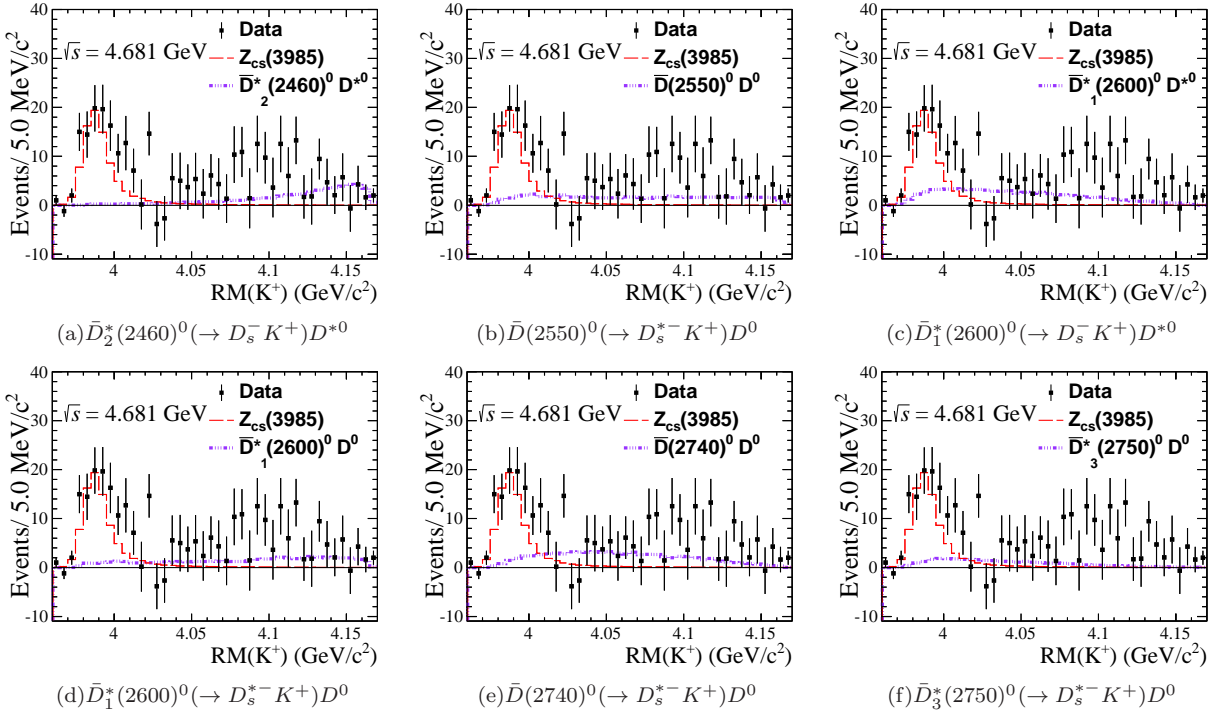


FIG. 4. K^+ recoil-mass spectra in data with the WS background contributions subtracted, and MC simulations of the excited D^{**} states in $e^+e^- \rightarrow \bar{D}^{**0}D^{(*)0}$. The $Z_{cs}(3985)^-$ shape is normalized to the yields observed in data and the shape of the \bar{D}^{**0} states is arbitrarily scaled.

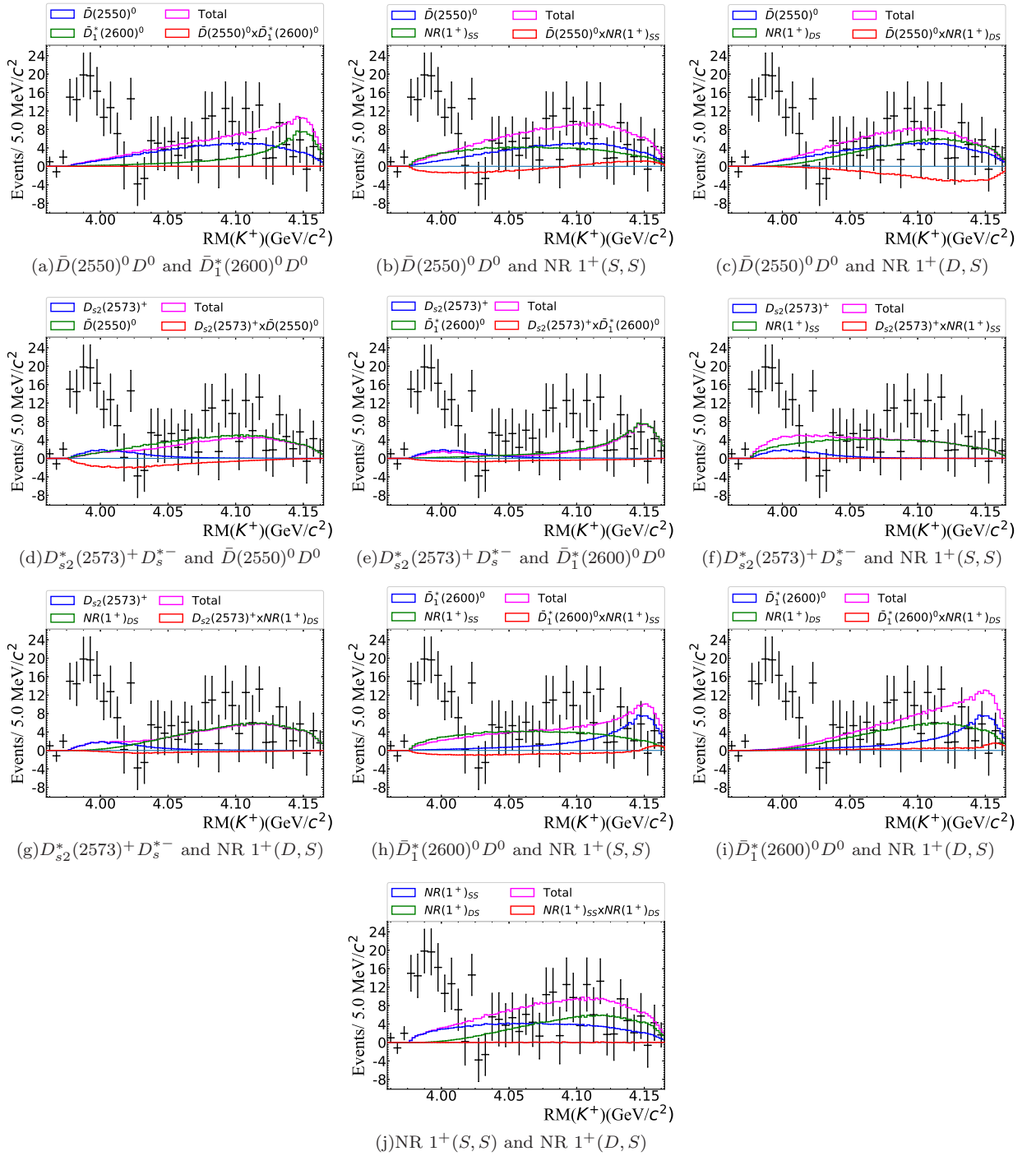


FIG. 5. K^+ recoil-mass spectra in data with the WS background contributions subtracted, and MC simulations of two possible background processes for the $K^+D_s^{*-}D^0$ final state, whose interferences are taken into account. The interference effect is tuned to be largest around $4.0 \text{ GeV}/c^2$. In the non-resonant (NR) process, the angular momentum ($L_{K^+X}, L_{D_s^{*-}D^0}$) denotes the angular momentum between K^+ and $X_{D_s^{*-}D^0}$, and D_s^{*-} and D^0 in the $e^+e^-(X_{D_s^{*-}D^0})$ rest frame, respectively. Individual contributions are scaled according to the observed yields in the control samples.

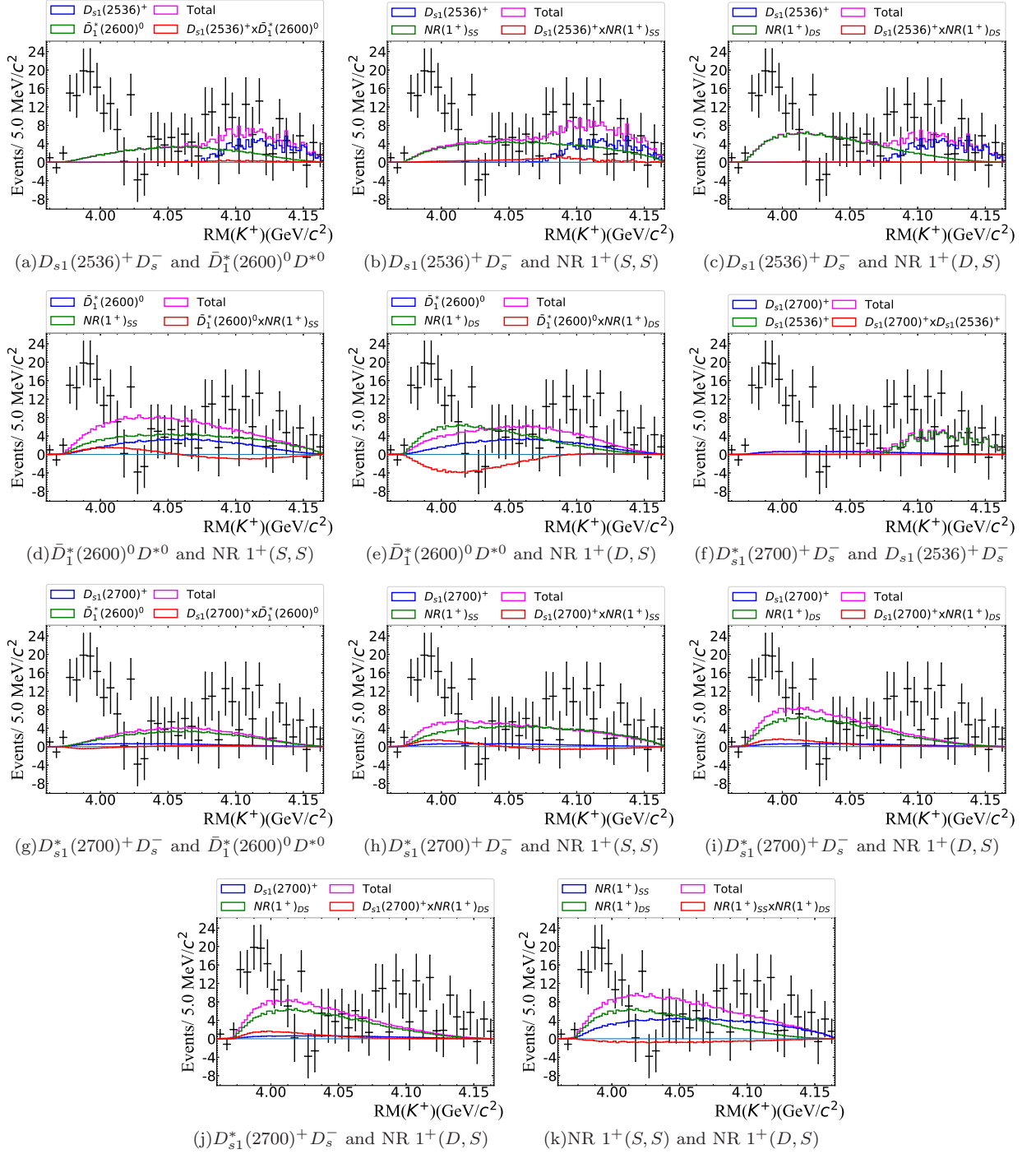


FIG. 6. K^+ recoil-mass spectra in data with the WS background contributions subtracted, and MC simulations of two possible background processes for the $K^+ D_s^- D^{*0}$ final state, whose interferences are taken into account. The interference effect is tuned to be largest around $4.0 \text{ GeV}/c^2$. In the non-resonant (NR) process, the angular momentum ($L_{K^+X}, L_{D_s^- D^{*0}}$) denotes the angular momentum between K^+ and $X_{D_s^- D^{*0}}$, and D_s^- and D^{*0} in the $e^+e^-(X_{D_s^- D^{*0}})$ rest frame, respectively. Individual contributions are scaled according to the observed yields in the control samples.

Appendix C: Systematics uncertainties

Sources of systematic uncertainties on the measurement of the $Z_{cs}(3985)^-$ resonance parameters and the cross section are studied, in which the main sources include the mass scaling, detector resolution, the signal model, background models and the input cross-section line shape for $\sigma^B(e^+e^- \rightarrow K^+Z_{cs}(3985)^-)$.

We select a control sample of $e^+e^- \rightarrow D_{s1}(2536)^+D_s^{*-} \rightarrow K^+D^{*0}D_s^{*-}$ at $\sqrt{s} = 4.681$ GeV by detecting K^+D^{*0} with $D^{*0} \rightarrow \pi^0D^0$, $D^0 \rightarrow K^-\pi^+$, $K^-\pi^+\pi^0$ as well as $K^-\pi^+\pi^+\pi^-$ with a missing D_s^{*-} in the final state to study the mass scaling of the recoil mass of the low-momentum bachelor K^+ . We fit the D_s^{*-} peak in the spectra of the recoil mass of K^+D^{*0} , where the D_s^{*-} signal is modeled with a MC-determined signal shape convolved with a Gaussian function to represent a potential difference between data and MC simulation. The fitted Gaussian parameters are determined to be $\mu = -0.2 \pm 0.5$ MeV/ c^2 and $\sigma_{\text{upper}} < 1.43$ MeV (68% C.L.), which are used to determine the systematic effects due to mass scaling and detection resolution. After incorporating the evaluated detection resolution difference up to the upper uncertainty, we find the maximum change on the result of the fitted width to be 1.0 MeV.

In this work the two Z_{cs} signal processes are difficult to distinguish due to the partial-reconstruction method and the limited sample size. Hence, without any a priori knowledge, we vary the BF ratio f in the range from 0.2 to 0.8, corresponding to the standard deviation of a uniform distribution from 0 to 1. We find the resulting changes on the mass and width to be 0.2 MeV/ c^2 and 1.0 MeV, respectively. In the nominal fit, we assume that the spin-parity of the $Z_{cs}(3985)^-$ is 1^+ and that the relative momentum between K^+ and $Z_{cs}(3985)^-$ in the rest frame of the e^+e^- system and the relative momentum between $D_s^-(D_s^{*-})$ and $D^{*0}(D^0)$ in $Z_{cs}(3985)^-$ system are both in an S -wave state, denoted as $1^+(S, S)$. This hypothesis can only be verified by an amplitude analysis of the signal final states, which is not feasible with the current statistics. Therefore, as systematic variations, we test the assumptions of spin-parity and angular momentum with $1^+(D, S)$, $0^-(P, P)$, $1^-(P, P)$ and $2^-(P, P)$ configurations. These tests give maximum changes of 1.0 MeV/ c^2 in the mass and 2.6 MeV in the width. The systematic uncertainty related to the combinatorial background is estimated by varying both the sideband yield within its uncertainties and the background parametrization; the quadrature sums of each largest difference from the nominal fit are 0.5 MeV/ c^2 and 0.5 MeV for the mass and width, respectively, which are taken as the systematic uncertainties. The efficiency curves adopted in the resonance fit are varied within the uncertainties of their parametrizations, and the differences of 0.1 MeV/ c^2 in mass and 0.2 MeV in width to the nominal fit are taken as the related systematic uncertainty.

Any potential effects of the known $D_{(s)}^{**}$ states (as listed in Table I) on the measurements are evaluated. We vary the size of the D_s^{**+} and $\bar{D}_3^*(2750)^0$ background components within their uncertainties in the fit and take the variations as systematic uncertainties. For the known \bar{D}^{**0} states, which have $RM(K^+)$ distributions similar to that of the NR signal, the fit is repeated with each state as an additional component with its shape taken from MC simulation and the yield as a free parameter. To further check the $\bar{D}_1^*(2600)^0$ component, we remove the NR component from the simultaneous fit. The ratio $\mathcal{B}(\bar{D}_1^*(2600)^0 \rightarrow D_s^-K^+)/\mathcal{B}(\bar{D}_1^*(2600)^0 \rightarrow D^-\pi^+)$ then increases from 0.00 ± 0.02 to 0.12 ± 0.02 . We evaluate the quadrature sum of the mass and width differences between each of the results from these alternative fits with respect to the nominal fit and assign the quadrature sums as related systematic uncertainties of 1.0 MeV/ c^2 for the mass and 3.4 MeV for the width. We vary the input Born cross section $\sigma^B(e^+e^- \rightarrow K^+Z_{cs}(3985)^-)$ within the uncertainties and repeat the signal extraction, which gives a maximum change of 0.6 MeV/ c^2 for the mass and 1.7 MeV for the width.

Other systematic effects mostly influence the measurement of the cross section. Average uncertainties associated with the tracking, PID and K_S^0 reconstruction efficiencies are estimated to be 3.6%, 3.6% and 0.4%, respectively. The efficiency of the $RM(K^+D_s^-)$ requirement is re-estimated by changing the MC-simulated resolution according to the observed difference with respect to data and the resulting change is taken as the systematic uncertainty on the cross section. The integrated-luminosity uncertainty, measured with large-angle Bhabha events, is estimated to be 1%. The uncertainties on the quoted BFs for the involved decays [30] are included as part of the systematic uncertainty.

Table II summarizes the systematic uncertainties on the cross sections at $\sqrt{s}=4.628, 4.641, 4.661, 4.681$ and 4.698 GeV.

TABLE II. Summary of systematic uncertainties on the cross sections at different energy points. The total systematic uncertainty corresponds to a quadrature sum of all individual items.

Source	$\sigma_{4.628}\mathcal{B}(\%)$	$\sigma_{4.641}\mathcal{B}(\%)$	$\sigma_{4.661}\mathcal{B}(\%)$	$\sigma_{4.681}\mathcal{B}(\%)$	$\sigma_{4.698}\mathcal{B}(\%)$
Tracking	3.6	3.6	3.6	3.6	3.6
Particle ID	3.6	3.6	3.6	3.6	3.6
K_S^0	0.4	0.4	0.4	0.4	0.4
$RM(K^+D_s^-)$	4.0	0.3	0.4	0.6	0.2
Resolution	0.2	1.0	1.9	1.1	0.8
f factor	7.8	7.7	6.7	6.4	5.9
Signal model	20.5	14.4	16.6	21.9	11.2
Backgrounds	54.8	5.9	12.0	3.1	7.8
Efficiencies	0.2	0.2	0.2	0.5	0.1
$D_{(s)}^{**}$ states	47.1	82.2	35.3	15.7	35.3
$\sigma^B(K^+Z_{cs}(3985)^-)$	11.9	5.7	22.1	13.4	32.1
Luminosity	1.0	1.0	1.0	1.0	1.0
Input BFs	2.7	2.7	2.7	2.7	2.7
total	76.8	84.5	47.3	31.5	50.3

Appendix D: Fit results based on three subsets of data set at $\sqrt{s} = 4.681$ GeV

To avoid potential bias, the analysis strategy is firstly implemented and validated using the first one-third of data set at $\sqrt{s} = 4.681$ GeV, where the fit result is shown in Fig. 7(left) and given in Table III. Afterward, we split the two-thirds of data into two parts for consistency check by implementing the same fit procedures, the results of which are depicted in Fig. 7(middle) and (right). The corresponding numerical results are listed in Table III. The fitted resonance parameters between the 1st and 3rd one-third of data set are consistent within statistical uncertainty, while the comparison between the 1st and 2nd one-third of data set shows that the fitted masses and widths are in agreement within 1.5σ and 1.0σ , respectively. Overall, the three sets of fit results are compatible and we can assume they are due to the same source. Hence, the three parts of data at $\sqrt{s} = 4.681$ GeV are combined to obtain the nominal fit results listed in Table III.

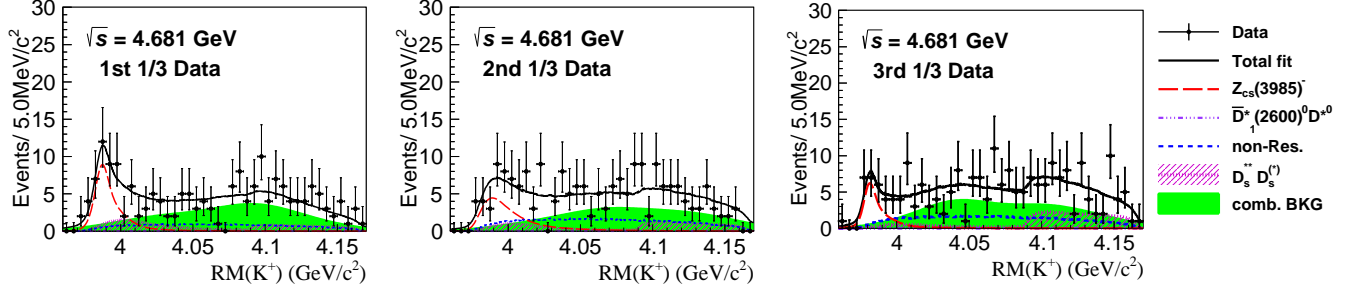


FIG. 7. Fit to the K^+ recoil mass spectra in the first (left), second (middle) and third (right) one-third of data set at $\sqrt{s} = 4.681$ GeV.

TABLE III. Fit results of the $Z_{cs}(3985)^-$ resonance parameters and cross sections based on the first, second and third one-third of data set at $\sqrt{s} = 4.681$ GeV.

Data set	Mass (MeV/c^2)	Width (MeV)	$\sigma_{4.681} \cdot \mathcal{B}(\text{pb})$	Statistical Significance
1st one-third	$3987.0^{+2.1}_{-2.4}$	$6.9^{+6.1}_{-4.1}$	$5.1^{+1.4}_{-1.2}$	4.9σ
2nd one-third	$3990.2^{+5.6}_{-5.5}$	$24.2^{+31.0}_{-12.4}$	$5.0^{+2.3}_{-1.8}$	2.9σ
3rd one-third	$3980.9^{+2.0}_{-2.2}$	$4.7^{+9.9}_{-4.7}$	$2.8^{+1.2}_{-1.0}$	3.9σ
nominal	$3985.2^{+2.1}_{-2.0}$	$13.8^{+8.1}_{-5.2}$	$4.4^{+0.9}_{-0.8}$	6.3σ

Appendix E: Calculation of the pole mass and width

The pole position $m_{\text{pole}}(Z_{cs}(3985)^-) - i\frac{\Gamma_{\text{pole}}(Z_{cs}(3985)^-)}{2}$ is determined by solving the equation

$$\begin{cases} M^2 - m_0^2 + im_0(f\Gamma_1(M) + (1-f)\Gamma_2(M)) = 0, \\ \Gamma_1(M) = \Gamma_0 \cdot \frac{p_1}{p_1^*} \cdot \frac{m_0}{M}, \\ \Gamma_2(M) = \Gamma_0 \cdot \frac{p_2}{p_2^*} \cdot \frac{m_0}{M}, \end{cases} \quad (\text{E1})$$

where the input values of m_0 and Γ_0 are taken from the simultaneous fit. The resonance mass is above the mass thresholds of the two coupled channels and the pole position is taken from Riemann sheet III defined in Ref. [37]. To properly account for their correlations, a Monte-Carlo method is adopted, in which pseudo data of m_0 and Γ_0 are generated according to the correlation matrix to calculate the pole position.